

Received: 6 December 2021 Revised: 14 January 2022 Accepted: 18 January 2022

# Tuning the moisture stability of multiphase $\beta$ -Li<sub>3</sub>PS<sub>4</sub> solid electrolyte materials

Xin Lu<sup>1,2,†</sup> | Osmane Camara<sup>1,†</sup> | Zigeng Liu<sup>1</sup> | Anna Windmüller<sup>1</sup> | Chih-Long Tsai<sup>1</sup> | Hermann Tempel<sup>1</sup> | Shicheng Yu<sup>1</sup> | Hans Kungl<sup>1</sup> | Rüdiger-A. Eichel<sup>1,2,3</sup>

# Correspondence

Shicheng Yu, Institut für Energie- und Klimaforschung (IEK-9: Grundlagen der Elektrochemie), Forschungszentrum Jülich, Jülich, D-52425, Germany. Email: s.yu@fz-juelich.de

# Funding information

Bundesministerium für Bildung und Forschung (BMBF), Grant/Award Number: 13XP0258B; High Performance Solid-State Batteries (HIPSTER)

# Abstract

Efficiently improving the moisture stability of β-Li<sub>3</sub>PS<sub>4</sub> materials could significantly reduce production costs and eventually enable the mass application. Nanoporous multiphase  $\beta$ -Li<sub>3</sub>PS<sub>4</sub> materials prepared via solvent-assistant routes usually contain solvent or solvent decomposition segments associated with the amorphous Li<sub>3</sub>PS<sub>4</sub> phase in their structures. Herein, the solvent ethyl propionate (EP) remains in the  $\beta$ -Li<sub>3</sub>PS<sub>4</sub> even after 220 h of annealing at 220°C. The possibility of tuning the moisture stability of  $\beta$ -Li<sub>3</sub>PS<sub>4</sub> by adjusting the content of the solvent is investigated by environmental scanning electron microscopy (ESEM) combined with other structural analysis techniques. The results demonstrated that the hydrogen-containing amorphous Li<sub>3</sub>PS<sub>4</sub> not only stabilizes the  $\beta$ -phase at room temperature but also improves the moisture stability of the material. Although the rapid hydrolysis occurs on the surface of solvent-containing  $\beta$ -Li<sub>3</sub>PS<sub>4</sub> materials under ambient conditions within 10 s, with 4 wt% EP content, the material can be exposed to 1.6% relative humidity (R.H.) for at least 8 h without any structural or microstructural change. Even with the lower amount of EP (1.2 wt%) in the Li<sub>3</sub>PS<sub>4</sub> structure, the material can withstand 1% R.H. for more than 8 h, which allows the material to be manufactured in a dry room. Our observation proposes a simple method to slightly modify the moisture stability of  $\beta$ -Li<sub>3</sub>PS<sub>4</sub> to match the different manufacturing conditions.

#### KEYWORDS

ambient stability, microstructure, moisture stability, solvent-containing Li<sub>3</sub>PS<sub>4</sub>, β-Li<sub>3</sub>PS<sub>4</sub>

# 1 | INTRODUCTION

Lithium thiophosphates are considered as promising solidstate electrolyte candidates for solid-state batteries as an alternative to current lithium-ion batteries because they possess sufficient ionic conductivity in the order of  $10^{-7}$ –  $10^{-4}$  S cm<sup>-1</sup> at room temperature and are highly ductile, which allows easy fabrication by cold pressing.<sup>[1]</sup> Among lithium thiophosphates, the metastable  $\beta$ -Li<sub>3</sub>PS<sub>4</sub> polymorph synthesized via solvent-assistant routes exhibits

This is an open access article under the terms of the Creative Commons Attribution-NonCommercial License, which permits use, distribution and reproduction in any medium, provided the original work is properly cited and is not used for commercial purposes.

© 2022 The Authors. *Electrochemical Science Advances* published by Wiley-VCH GmbH.

<sup>&</sup>lt;sup>1</sup> Institut für Energie- und Klimaforschung (IEK-9: Grundlagen der Elektrochemie), Forschungszentrum Jülich, Jülich, Germany

<sup>&</sup>lt;sup>2</sup> Institut für Materialien und Prozesse für elektrochemische Energiespeicher- und wandler, RWTH Aachen University, Aachen, Germany

<sup>&</sup>lt;sup>3</sup> Institut für Energie- und Klimaforschung (IEK-12: Helmholtz-Institute Münster, Ionics in Energy Storage), Forschungszentrum Jülich, Münster, Germany

<sup>&</sup>lt;sup>†</sup>These authors contributed equally to this work

Chemistry Europe

European Chemical Societies Publishing

extraordinary room temperature ionic conductivities up to 0.9 mS cm $^{-1}$ .[2–5]

In 2013, Liu et al. developed a pioneering three-step solvent-assistant method in tetrahydrofuran (THF) for the preparation of nanoporous  $\beta$ -Li<sub>3</sub>PS<sub>4</sub>,<sup>[3]</sup> which provided an easily scalable manufacturing route and raised the prospect of mass production of solid electrolytes.<sup>[6,7]</sup> Later, EP is also widely used for the synthesis of this material<sup>[7–9]</sup> because it was listed as a non-toxic solvent by the US Food and Drug Administration (Class 3) and can promote the reaction between Li<sub>2</sub>S and P<sub>2</sub>S<sub>5</sub> through the ester group.<sup>[4]</sup>

The origin of such high conductivity of  $\beta$ -Li<sub>3</sub>PS<sub>4</sub> is the result of synergistic ionic conduction in multiple phases. [2,10,11] The "so-called"  $\beta$ -Li<sub>3</sub>PS<sub>4</sub> prepared by wet chemical route is actually a porous multiphase material composed of crystalline  $\beta$ -Li<sub>3</sub>PS<sub>4</sub>, amorphous Li<sub>3</sub>PS<sub>4</sub>, and hydrogen-containing Li<sub>3</sub>PS<sub>4</sub> (e.g., Li<sub>3</sub>PS<sub>4</sub>·2THF).<sup>[11]</sup> Marchini et al. investigated the ionic conductivity of these phases by tuning the crystallinity and solvent content in nanoporous β-Li<sub>3</sub>PS<sub>4</sub> materials and found that the amorphous phase is the most conductive among others. [11] Although the hydrogen-containing Li<sub>3</sub>PS<sub>4</sub> seems to be detrimental to the ionic conductivity, [12] this component can be completely removed from the structure only at about 400°C, which is far above what is normally used for the synthesis of nanoporous  $\beta$ -Li<sub>3</sub>PS<sub>4</sub> (160–300°C).<sup>[10]</sup> The remaining residual solvent or solvent decomposition segments in the products indirectly contribute to the overall ionic conductivity by helping to maintain the large surface area of the material and thus stabilizing the  $\beta$ -phase at room temperature.[10]

Despite its simple fabrication method and high ionic conductivity,  $\beta$ -Li<sub>3</sub>PS<sub>4</sub> is known to be unstable under ambient conditions and decomposes rapidly. [13-15] β-Li<sub>3</sub>PS<sub>4</sub> undergoes hydrolysis leading to a final critical reaction that produces H<sub>2</sub>S gas and Li<sub>3</sub>PO<sub>4</sub>. [14-17] Based on the hard and soft acids and bases (HSAB) theory, the fast hydrolysis of thiophosphate materials is due to the fact that oxygen is a hard base that reacts preferentially with the hard acid P and replaces the soft base S.<sup>[18]</sup> Therefore, proper evaluation and suppression of this reaction could be the access for the mass production of  $\beta$ -Li<sub>3</sub>PS<sub>4</sub>. Inspired by these, instead of stabilizing P or S by substitution or doping, [18-27] which alters the original structure and increases the complexity and cost of synthesis, a simple adjustment of the content of hydrogen-containing Li<sub>3</sub>PS<sub>4</sub> could improve the air stability of  $\beta$ -Li<sub>3</sub>PS<sub>4</sub> to some extent. The residual solvent or solvent decomposition segments in the structure may bind with P and/or S, stabilizing the structure. Furthermore, hard bases (H<sub>2</sub>O) react preferentially with hard acid groups (e.g. H<sup>+</sup>) in the solvent.

In this work, porous  $\beta$ -Li<sub>3</sub>PS<sub>4</sub> materials content 1.2 and 4.0 wt% EP were respectively prepared by adjusting the

annealing time. Their structural and microstructural stabilities under ambient conditions, dry synthetic air, and various moisture contents were investigated by ESEM and X-ray diffraction (XRD) analysis. The microstructure deformation as the direct reflection of the rapid hydrolysis of  $\beta\text{-Li}_3\text{PS}_4$  was first time recorded and reported. Moreover, it is possible to change the solvent content by varying the annealing time to slightly adjust the moisture stability of  $\beta\text{-Li}_3\text{PS}_4$  to be applied to different fabrication conditions.

# 2 | RESULTS AND DISCUSSION

Two  $\beta$ -Li<sub>3</sub>PS<sub>4</sub> samples with high and low EP content were prepared using the methods described in the supporting information. These samples were heated at 220°C and are denoted as LPS<sub>4h</sub> for the sample heated for 4 h and LPS<sub>220h</sub> for the sample heated for 220 h. Powder XRD measurements were carried out in order to investigate the crystal structure and phase purity of the prepared samples. As shown in Figure 1a, all the reflexes are assigned to orthorhombic space group Pnma that indexed to the standard  $\beta$ -Li<sub>3</sub>PS<sub>4</sub> pattern (ICSD No. 180319), indicating that this material is successfully formed in both cases. The peak width of the XRD patterns is narrowed for the LPS<sub>220h</sub> sample, indicating the crystallinity increased after heating for a longer time. Moreover, the XRD patterns of the asprepared powders show a distinct background, probably related to the presence of amorphous Li<sub>3</sub>PS<sub>4</sub> and caused by the Scotch Magic tape used to prevent air access to the sample. According to the recent reports, the β-Li<sub>3</sub>PS<sub>4</sub> prepared by wet chemistry is possibly a "multiphasic material".[10,11] Marchini et al confirmed the presence of a striking maximum of 52% of additional amorphous materials in the  $\beta$ -Li<sub>3</sub>PS<sub>4</sub> synthesized in THF, depending on the heating process.[11] The presence of the amorphous H-containing Li<sub>3</sub>PS<sub>4</sub> phase has been claimed as the reason to stabilize  $\beta$ -Li<sub>3</sub>PS<sub>4</sub> at room temperature. [10] Here, the syntheses are carried out in EP which has a much higher boiling point than THF, it is possible that the EP is still present in the structure of Li<sub>3</sub>PS<sub>4</sub> even though the samples were dried at 90°C under 500 Pa for two days and subsequently heated at 220°C for a maximum of 220 h.

The presence of EP in the prepared LPS<sub>4h</sub> and LPS<sub>220h</sub> is confirmed by the attenuated total reflectance infrared spectroscopy (ATR-IR), as the results are shown in Figure 1b. The IR spectrum of EP shows C-H alkyl stretching vibrations in the wavenumber range of 2860–3000 cm<sup>-1</sup>, C = O stretching vibrations at 1731 cm<sup>-1</sup>, and C-O stretching vibrations at 1182 cm<sup>-1</sup>. The other peaks at the wavenumbers  $\sim$ 1500–400 cm<sup>-1</sup> are considered the unique set of complex overlapping vibrations of the atoms of the EP molecular. These characteristic peaks

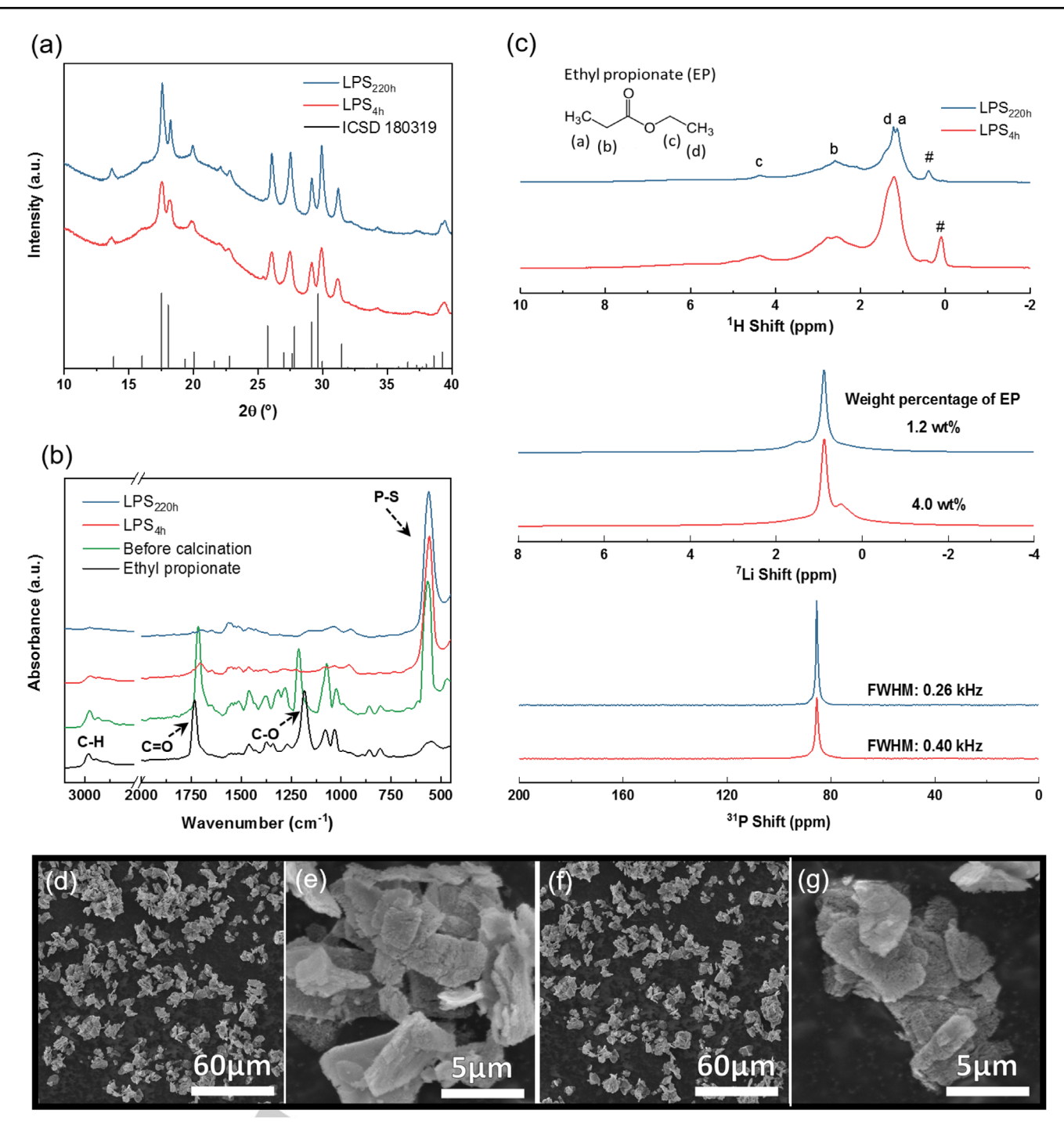


FIGURE 1 (a) X-ray diffraction (XRD) pattern of LPS<sub>4h</sub> and LPS<sub>220h</sub> along with reference XRD pattern (ICSD 180319). (b) Attenuated total reflectance infrared spectroscopy (ATR-IR) spectra of ethyl propionate (EP), Li<sub>3</sub>PS<sub>4</sub> before calcination, β-Li<sub>3</sub>PS<sub>4</sub> heated at 220°C for 4 and 220 h, respectively. (c) <sup>1</sup>H NMR, <sup>7</sup>LI NMR, and <sup>31</sup>P NMR spectra of LPS<sub>4h</sub> and LPS<sub>220h</sub>. Scanning electron microscopy (SEM) images of as-prepared LPS<sub>4h</sub> powders (d, e) and LPS<sub>220h</sub> powders (f, g).

of EP are observed with different intensities and slightly shifted locations in the results of all three  $\text{Li}_3\text{PS}_4$  samples with or without calcination. The IR spectrum of pristine  $\text{Li}_3\text{PS}_4$  presented clear peak shifts at the wavenumbers ~1500–400 cm<sup>-1</sup>, and enhanced intensity at 1311, 1280, and 1070 cm<sup>-1</sup> compared with that of EP. These could be due to the interaction between the remaining EP with

Li<sub>3</sub>PS<sub>4</sub> after drying at 90°C. In addition, like for both 220°C heated samples, the IR spectrum of the pristine Li<sub>3</sub>PS<sub>4</sub> presented a clear characteristic peak of the PS<sub>4</sub> group at the wavenumber of  $\sim$ 550 cm<sup>-1</sup>, indicating the P-S bond is already formed before high-temperature treatment. After heating at 220°C, the relative intensities of C = O and C-O peaks presented in the IR spectra of LPS<sub>4h</sub> and LPS<sub>220h</sub>

Chemistry Europe

European Chemical Societies Publishing

significantly decreased compared with that of the pristine sample, indicating EP may be (partially) decomposed in the heating process. The low intensity of the characteristic peaks of EP in the IR spectrum of  $LPS_{220h}$  signifies a relatively low content of the EP segments in the structure. Since IR is mostly used for qualitative identification, the quantification of EP in  $LPS_{4h}$  and  $LPS_{220h}$  is performed by nuclear magnetic resonance spectroscopy (NMR).

To quantify the EP amount and to further elucidate the structural information of as-prepared samples. <sup>1</sup>H. <sup>7</sup>Li, and <sup>31</sup>P magic angle spinning NMRs were conducted. The presence of EP was further confirmed by <sup>1</sup>H NMR spectra of as-prepared LPS samples, in Figure 1c, with the four isotropic resonances corresponding to the four different H environments in EP. The broad and asymmetric line shape of the <sup>1</sup>H isotropic resonances is due to the lack of mobility of EP inside the LPS structure, likely leading to form an amorphous Li<sub>3</sub>PS<sub>4</sub>·xEP phase beside crystal β-Li<sub>3</sub>PS<sub>4</sub> phase. Moreover, an additional peak (#) is also observed, which is most likely a -CH3 group originating from the partially decomposed segments of EP. This is consistent with the ATR-IR results. 7Li NMR spectra of LPS<sub>4h</sub> and LPS<sub>220h</sub> samples show three isotropic resonances at 0.87, 1.30, and 0.50 ppm, which can be tentatively assigned to the three Li sites: the fully occupied tetrahedral site (8d), the partially occupied octahedral site (4b) and the partially occupied tetrahedral site (4c), in the  $\beta$ -Li<sub>3</sub>PS<sub>4</sub> structure, respectively. Additionally, compared with the longer heated LPS<sub>220h</sub> sample, the relative intensity ratio of the partially occupied octahedral site (4b) decreased while the partially occupied tetrahedral site (4c) is increased in the LPS<sub>4h</sub> sample, implying that Li ions on the partially occupied octahedral site (4b) are more thermally stable than that on the partially occupied tetrahedral site (4c). Furthermore, the weight ratio of LPS: EP in the samples (Figure 1c) was determined with an external reference Li<sub>1.3</sub>Al<sub>0.3</sub>Ti<sub>1.7</sub>(PO<sub>4</sub>)<sub>3</sub>. LPS<sub>220h</sub> has a lower weight percentage of EP of 1.2% compared with that of LPS<sub>4h</sub>, 4.0%, which is in agreement with the <sup>1</sup>H NMR spectra. Therefore, except for the crystal  $\beta$ -Li<sub>3</sub>PS<sub>4</sub>, there are about 1.2% and 4.0% of amorphous H-containing Li<sub>3</sub>PS<sub>4</sub>·xEP present in LPS<sub>4h</sub> and LPS<sub>220h</sub>, respectively. <sup>31</sup>P NMR showed an isotropic resonance at 85.5 ppm, which is assigned to the PS<sub>4</sub> tetrahedra. In addition, the full width half maximum (FWHM) of LPS<sub>220h</sub> is 0.26 kHz compared with LPS<sub>4h</sub> which has an FWHM of 0.40 kHz, indicating the local environment of <sup>31</sup>P in LPS<sub>220h</sub> is more symmetric than that in LPS<sub>4h</sub>. This is consistent with the XRD results. The NMR results indicate that as the heating time increases the amount of EP decreases while the crystallinity of  $\beta$ -Li<sub>3</sub>PS<sub>4</sub> improved.

To accurately record the morphology of the samples, an airtight SEM transfer module (Figure S1a) is used as a sam-

ple holder so that the samples can be transferred directly from a glovebox to the ESEM chamber without contamination from the atmosphere. Moreover, the parameters for SEM measurement are optimized to eliminate charging effects, as shown in Figure S1b and discussed in detail in the supporting information. All SEM images shown in the following are acquired at an accelerating voltage of 1 kV with 64 times line integration and a low dwell time of 50 ns. The SEM images of as-prepared LPS<sub>4h</sub> and LPS<sub>220h</sub> powders are shown in Figure 1d–g, respectively. The particles displayed a flake-like structure with sizes in the range of 5  $\mu$ m in length, 3  $\mu$ m in width, and 200–300 nm in thickness. Besides, the LPS<sub>4h</sub> and LPS<sub>220h</sub> particles are porous, which is due to the effects of solvent removal.

The LPS<sub>4h</sub> and LPS<sub>220h</sub> powders were, respectively, pressed into pellets with a diameter of ~10 mm and then polished to remove the pressed skin. Benefited from low Li-S bond energy and a moderate Young's modulus of Li<sub>3</sub>PS<sub>4</sub>,<sup>[28]</sup> dense LPS<sub>4h</sub> and LPS<sub>220h</sub> pellets are formed by isostatic pressuring at room temperature. The average relative densities of LPS<sub>220h</sub> and LPS<sub>4h</sub> are 93.0% and 94.5%, respectively. Hence, the shape and density of the prepared β-Li<sub>3</sub>PS<sub>4</sub> samples are highly consistent with the solid electrolytes applied on the laboratory scale. The room temperature ionic conductivities of the pellets are calculated from the impedance spectra shown in Figure S2. Despite the slightly low density of LPS<sub>220h</sub>, its ionic conductivity is 0.15 mS cm<sup>-1</sup> which is 50% higher than that of LPS<sub>4h</sub> (0.1 mS cm<sup>-1</sup>), indicating that increasing the EP content negatively affect the ionic conductivity of LPS. The same is true for THF solvent reported previously.[11]

The initial morphology and relevant structure stability under ambient conditions ( $\sim$ 45% relative humidity, R.H.,  $\sim$ 1400 Pa of moisture) of the  $\beta$ -Li<sub>3</sub>PS<sub>4</sub> pellets consisting of low (LPS<sub>220h</sub>) and high (LPS<sub>4h</sub>) amounts of H-containing Li<sub>3</sub>PS<sub>4</sub> phase are investigated and revealed in Figure 2. The comparison of the morphological changes of the samples during the exposure time of 1 h can also be seen in Video S1. Before exposure to ambient conditions (images recorded at 0 s), the LPS<sub>220h</sub> and LPS<sub>4h</sub> pellets initially exhibited highly compacted structures. There are no pores or loose particles observed in the SEM images at the primary states of both samples but smooth surfaces with grooves of  $\sim$ 800 nm width in multiple directions as a result of polishing.

As presented in Figure 2 and Video S1, cracks appeared on the surfaces of both samples after only 10 seconds under ambient conditions, revealing the appearance of rapid chemical reaction(s). Interestingly, cracking begins in areas where grooves are present from polishing and then propagates out from these primary straight cracks over exposure time. Sulfide electrolytes undergo hydrolysis with moisture that produces  $\text{Li}_3\text{PO}_4$  and  $\text{H}_2\text{S}.^{[16,27]}$  The

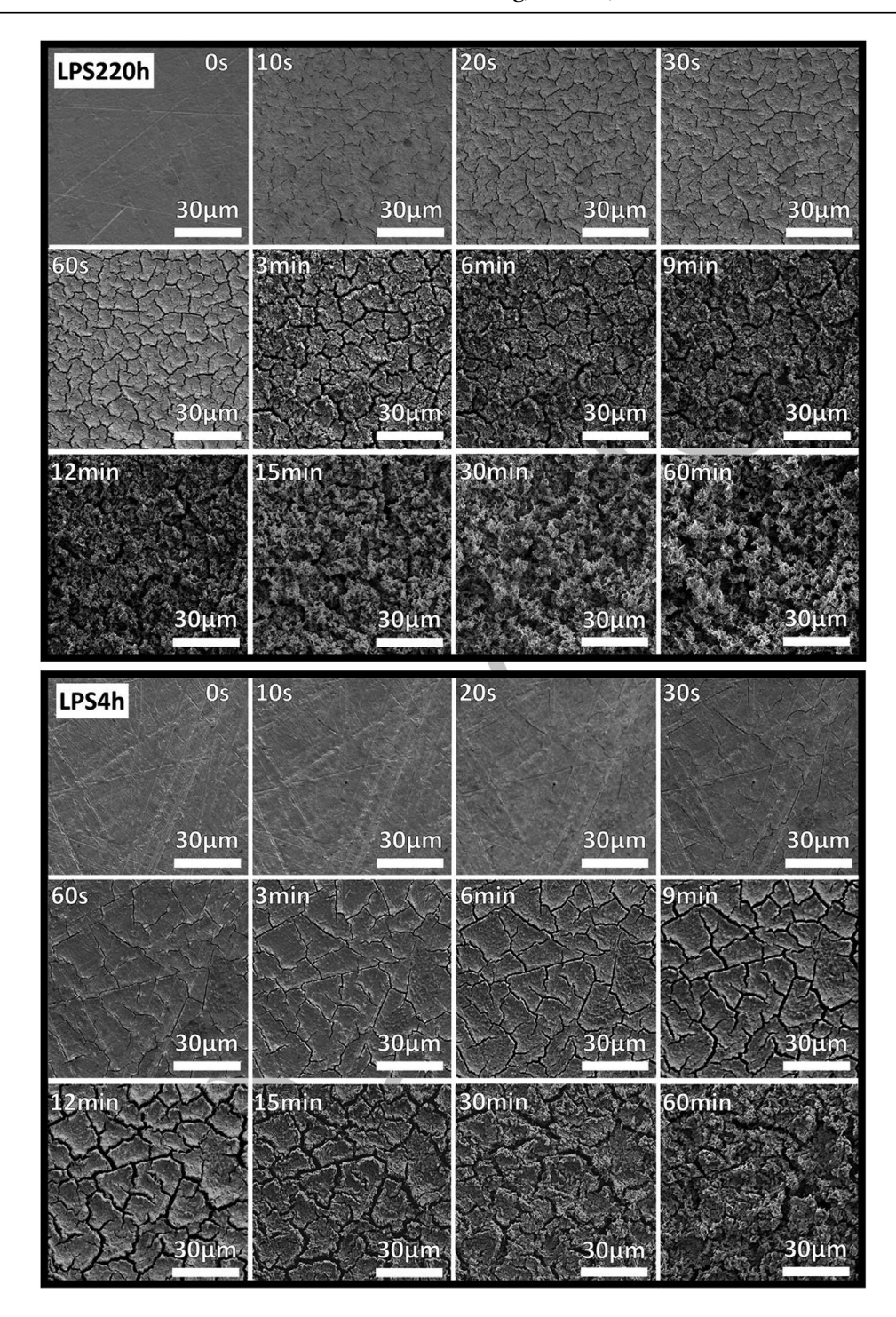


FIGURE 2 Scanning electron microscopy (SEM) images of  $LPS_{220h}$  and  $LPS_{4h}$  pellets at initial states and after exposure to the ambient environment after 10 s, 20 s, 30 s, 1 min, 3 min, 9 min, 12 min, 15 min, 30 min, and 60 min, respectively.

uptake of water by the sample together with the gas formation seems to be the reason for the cracking. Moreover, the pressure of the formed gases would cause cracks starting from the grooves due to the mechanical stress concentrations in these areas.

The noticeable difference between the structure decomposition processes of LPS $_{220h}$  and LPS $_{4h}$  is that the formation and growth of cracks are very fast in LPS $_{220h}$ , account-

ing for 4% surface coverage after 10 s and reached 25% after 150 s (cf. Figure 2 and area of the surface cracks as a function of exposure duration in Figure S3). These crack coverage values are reached by the high EP content  $\beta$ -Li<sub>3</sub>PS<sub>4</sub>, LPS<sub>4h</sub>, after much longer exposure periods of 80 s and 900 s, respectively. When the exposure time was further extended to 1 h in ambient conditions, the cracks in both samples developed and grew continuously, with

 $LPS_{4h}$  exhibiting better morphology stability compared to  $LPS_{220h}$  at all recorded times.

Figure S4 shows the surface XRD profiles of both pellets after exposure to ambient conditions for 1 h. The diffraction peaks of  $\beta$ -Li<sub>3</sub>PS<sub>4</sub> disappeared, remaining the peaks from various degraded components of oxides and sulfides, including Li<sub>2</sub>O, Li<sub>3</sub>P<sub>2</sub>O<sub>7</sub>, Li<sub>3</sub>PO<sub>4</sub>, Li<sub>4</sub>P<sub>2</sub>S<sub>6</sub>, Li<sub>2</sub>P<sub>2</sub>S<sub>6</sub>, and Li<sub>7</sub>PS<sub>4</sub>. These results suggested that in addition to the morphological changes on the sample surfaces, there is also a strong chemical degradation of the material. Besides, the initial LPS<sub>220h</sub> visually presented as a darker more saturated orange-brown when compared to that of LPS<sub>4h</sub>, this difference is attributed to the lower EP content in LPS<sub>220h</sub> (Figure S5).<sup>[29]</sup> After 1 h in the environment, both samples turned gray. The LPS<sub>220h</sub> pellet disintegrated into loose powders and could not maintain its structure, while the LPS<sub>4h</sub> pellet was able to maintain its pellet shape despite the deteriorated surface, as evidenced by the photos shown in Figure S5. The overall higher microstructure stability of LPS<sub>4h</sub> at ambient conditions could be due to the higher EP content in the material, which could combine with P or/and S and stabilize the structure. Moreover, according to the HSAB theory, the hard base (H<sub>2</sub>O) tends to interact with the hard acid. [18] The more EP in Li<sub>3</sub>PS<sub>4</sub>, the more weakly acidic methylene groups are in the structure, which could possibly eliminate the effects of moisture to some extent.

In addition to the rapid hydrolysis reaction of S and H in  $\text{Li}_3\text{PS}_4$  and moisture respectively, the  $\text{Li}_3\text{PS}_4$  materials are inherently extremely hygroscopic because of the intimate affinity between P and O from the moisture. Therefore, studying the effects of different moisture levels on  $\beta\text{-Li}_3\text{PS}_4$  could provide insight into the proper handling of these materials during manufacture and application.

To investigate the effects of moisture on the LPS $_{220h}$  and LPS $_{4h}$  pellets, different levels of humidity were introduced into the SEM chamber without carrier gas. After desired exposure times, imaging was performed after the moisture was removed from the chamber to avoid accelerated reactions between moisture and Li $_3$ PS $_4$  under high-speed electron bombardment. Such strong acceleration effects can be seen in Figure S6.

As demonstrated in Figure 3, the LPS $_{220h}$  sample with low EP content (more reactive under ambient conditions) was exposed to the moisture of 50 Pa (1.6% R.H.) in the ESEM chamber and allowed to interact for 8 h. This sample exhibited a small amount of cracking, equivalent to 0.6% of the surface area. This amount of cracking is the same value obtained under ambient conditions after 10 s. This indicates that the amount of moisture present in the environment plays an important role in the degradation process of LI $_3$ PS $_4$ . As such, another LPS $_{220h}$  pellet was tested at 30 Pa (1% R.H.). This sample showed no crack forma-

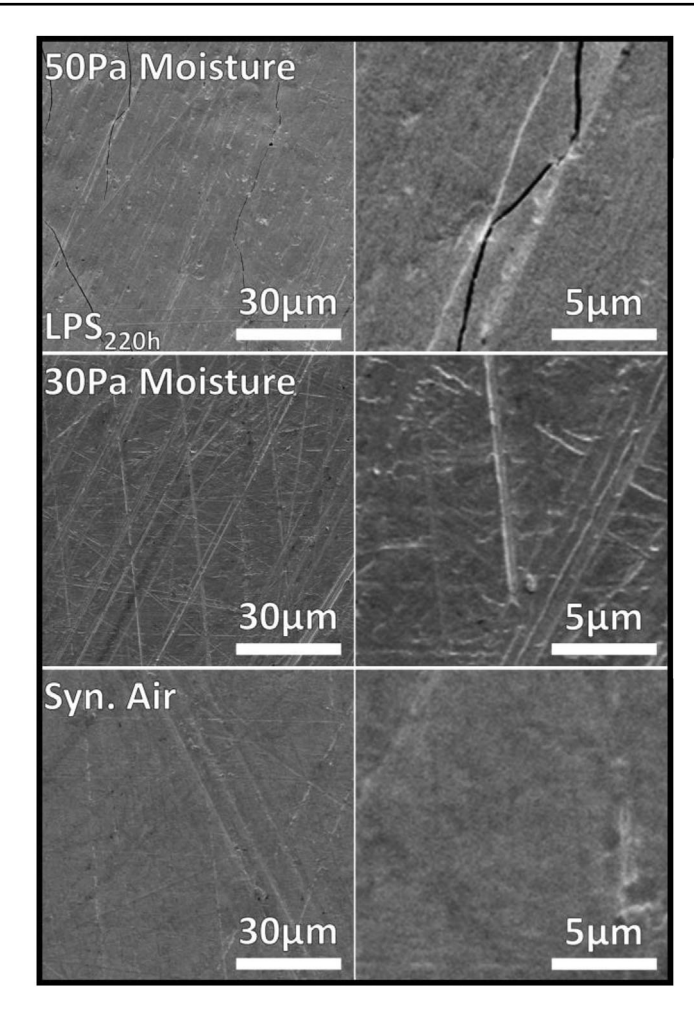
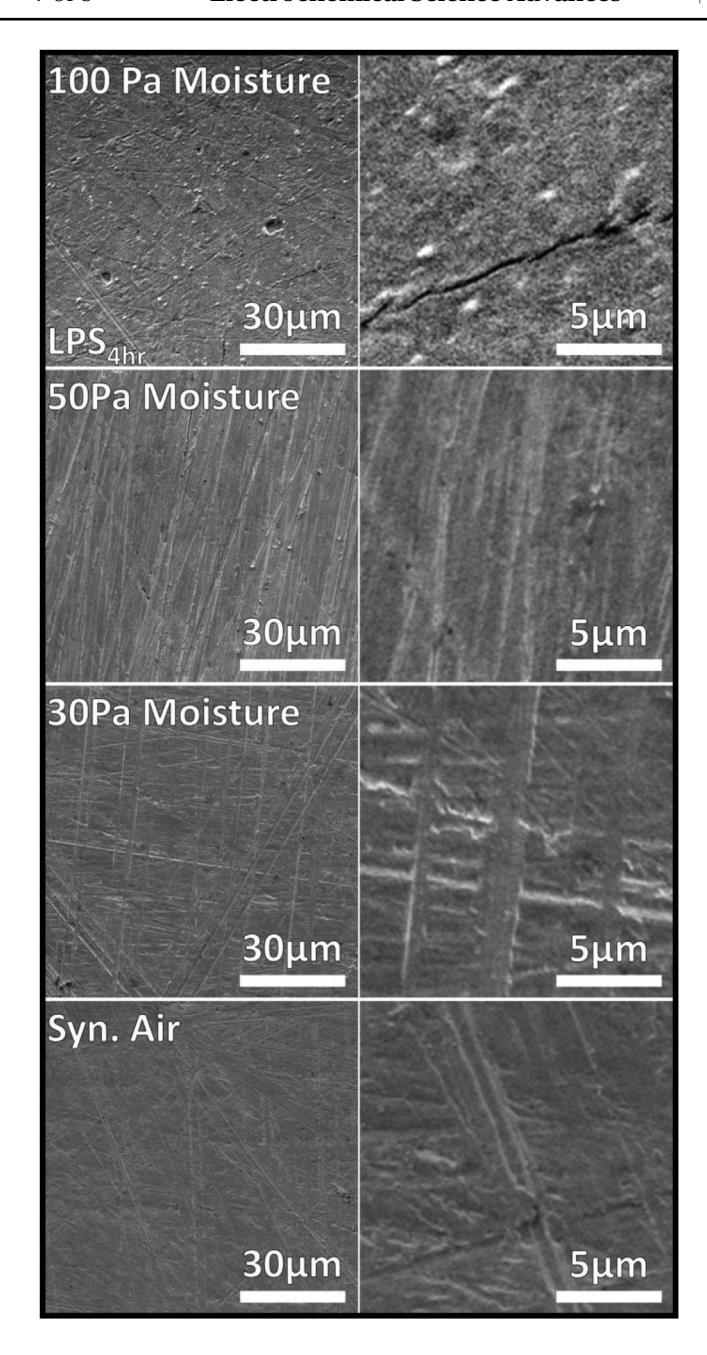


FIGURE 3 Scanning electron microscopy (SEM) images of LPS $_{220h}$  pellets after exposed to 50 and 30 Pa of moisture for 8 h, and 2000 Pa of synthetic dry air for 1 h.

tions after 8 h of interaction with a small amount of moisture (Figure 3). To confirm that gases in the ambient air were not responsible for the degradation of Li<sub>3</sub>PS<sub>4</sub>, dry synthetic air with ultra-low moisture ( $H_20 < 3$  ppm) was injected into the chamber until a pressure of 2000 Pa was reached. After 1 h, the surface showed no surface crack (Figure 3). XRD was carried out on all samples after exposure and a pellet exposed to dry synthetic airflow for one day. The results can be found in Figure S7. In line with the microstructure change, except for the sample exposed 8 h to 50 Pa moisture, all other samples showed no chemical decomposition. As shown in Figure 4, the LPS<sub>4h</sub> sample with high EP content exhibited better moisture resistivity than LPS<sub>220h</sub>. The samples exposed 8 h to 50 and 30 Pa moisture and 1 h to dry synthetic air show no cracking. Crack formation of 0.5% surface area is observed for the sample exposed to 100 Pa (3.2% R.H.) of moisture for 1 h, equivalent to the amounts of cracks formed under ambient conditions after 10 s. However, the formation of a small



**FIGURE 4** Scanning electron microscopy (SEM) image of LPS<sub>4h</sub> after exposure to 100 Pa of moisture for 1 h, 50 and 30 Pa of moisture for 8 h, and 2000 Pa of synthetic dry air for 1 h.

number of cracks is accompanied by significant structural changes, as indicated by the XRD results in Figure S8.

The analytical method presented in this work allows accuracy recording the microstructure of  $\text{Li}_3\text{PS}_4$  and direct observation of the rapid microstructural changes caused by the hydrolysis reaction without the influence of the electron beam. Moreover, the solvent-containing  $\text{Li}_3\text{PS}_4$  phase was confirmed to play a role in improving moisture resistance. Furthermore, the results provide insights into properly preparing and handling the  $\text{Li}_3\text{PS}_4$  materials. Instead of fabricating and applying  $\text{Li}_3\text{PS}_4$  inside an inert environ-

ment, work can be done instead in a dry room as it has been shown that even after a full day of exposure to ambient gases, the material is stable. By operating inside a dry room that typically has an R.H. under 1%, the process is greatly simplified and a reduction in the processing cost can be achieved.

#### 3 | CONCLUSION

The results demonstrate that hydrolysis causes the rapid crack formation and propagation of nanoporous multiphase  $\beta$ -Li<sub>3</sub>PS<sub>4</sub> materials consisting of crystalline  $\beta$ -Li<sub>3</sub>PS<sub>4</sub> and hydrogen-containing Li<sub>3</sub>PS<sub>4</sub>·xEP within a short exposure time of 10 s under ambient conditions. The hydrogen-containing Li<sub>3</sub>PS<sub>4</sub>·xEP plays a role in suppressing hydrolysis reaction to some extent. The LPS<sub>220h</sub> (1.2 wt% EP content) and LPS<sub>4h</sub> (4.0 wt% EP content) can bear at least an exposure time of 8 h in 1% and 1.6% R.H., respectively, with no structural or microstructural changes. This indicates that porous multiphase  $\beta$ -Li<sub>3</sub>PS<sub>4</sub> containing even a small amount of solvent can be synthesized and applied under dry room conditions without chemical modification such as doping or substitution of P or S.

#### **ACKNOWLEDGMENTS**

This work was financially supported by the project of "Materials and Components to Meet High Energy Density Batteries III" of the funding program "Excellent battery" from the Bundesministerium für Bildung und Forschung (BMBF) (Project No.: 13XP0258B), and the project "High Performance Solid-State Batteries" (HIP-STER) from "Ministerium für Kultur und Wissenschaft des Landes Nordrhein-Westfalen".

#### CONFLICT OF INTEREST

The authors declare that they have no conflict of interest.

# DATA AVAILABILITY STATEMENT

The data that support the findings of this study are available from the corresponding author upon reasonable request.

# ORCID

*Shicheng Yu* https://orcid.org/0000-0002-6619-3330

# REFERENCES

- H. Wang, Z. D. Hood, Y. Xia, C. Liang, J. Mater. Chem. A 2016, 4, 8091.
- 2. K. Homma, M. Yonemura, T. Kobayashi, M. Nagao, M. Hirayama, R. Kanno, *Solid State Ionics* **2011**, *182*, 53.
- Z. Liu, W. Fu, E. A. Payzant, X. Yu, Z. Wu, N. J. Dudney, J. Kiggans, K. Hong, A. J. Rondinone, C. Liang, *J. Am. Chem. Soc.* 2013, 135, 975.

Short Communication

doi.org/10.1002/elsa.202100208

- N. H. H. Phuc, M. Totani, K. Morikawa, H. Muto, A. Matsuda, Solid State Ionics 2016, 288, 240.
- H. D. Lim, X. Yue, X. Xing, V. Petrova, M. Gonzalez, H. Liu, P. Liu, J. Mater. Chem. A 2018, 6, 7370.
- A. Miura, N. C. Rosero-Navarro, A. Sakuda, K. Tadanaga, N. H. H. Phuc, A. Matsuda, N. Machida, A. Hayashi, M. Tatsumisago, Nat. Rev. Chem. 2019, 3, 189.
- K. Yamamoto, M. Takahashi, K. Ohara, N. H. H. Phuc, S. Yang, T. Watanabe, T. Uchiyama, A. Sakuda, A. Hayashi, M. Tatsumisago, H. Muto, A. Matsuda, Y. Uchimoto, *ACS Omega* 2020, 5, 26287.
- 8. N. H. H. Phuc, K. Morikawa, T. Mitsuhiro, H. Muto, A. Matsuda, *Ionics* **2017**, *23*, 2061.
- 9. Ö. U. Kudu, T. Famprikis, B. Fleutot, M. D. Braida, T. Le Mercier, M. S. Islam, C. Masquelier, *J. Power Sources* **2018**, *407*, 31.
- K. Kaup, L. Zhou, A. Huq, L. F. Nazar, J. Mater. Chem. A 2020, 8, 12446.
- F. Marchini, B. Porcheron, G. Rousse, L. Albero Blanquer, L. Droguet, D. Foix, T. Koç, M. Deschamps, J. M. Tarascon, Adv. Energy Mater. 2021, 11, 2101111.
- M. Takahashi, S. Yang, K. Yamamoto, K. Ohara, N. H. H. Phuc, T. Watanabe, T. Uchiyama, A. Sakuda, A. Hayashi, M. Tatsumisago, H. Muto, A. Matsuda, Y. Uchimoto, *Solid State Ionics* 2021, *361*, 115568.
- 13. H. Muramatsu, A. Hayashi, T. Ohtomo, S. Hama, M. Tatsumisago, *Solid State Ionics* **2011**, *182*, 116.
- H. M. Chen, C. Maohua, S. Adams, *Phys. Chem. Chem. Phys.* 2015, 17, 16494.
- A. Neveu, V. Pelé, C. Jordy, V. Pralong, J. Power Sources 2020, 467, 228250.
- 16. T. Ohtomo, A. Hayashi, M. Tatsumisago, K. Kawamoto, *J. Mater. Sci.* **2013**, *48*, 4137.
- K. Kaup, J. D. Bazak, S. H. Vajargah, X. Wu, J. Kulisch, G. R. Goward, L. F. Nazar, *Adv. Energy Mater.* 2020, *10*, 1902783.
- G. Sahu, Z. Lin, J. Li, Z. Liu, N. Dudney, C. Liang, *Energy Environ. Sci.* 2014, 7, 1053.
- R. Matsuda, T. Kokubo, N. H. H. Phuc, H. Muto, A. Matsuda, Solid State Ionics 2020, 345, 115190.

- H. Wang, Y. Chen, Z. D. Hood, G. Sahu, A. S. Pandian, J. K. Keum, K. An, C. Liang, *Angew. Chemie Int. Ed.* 2016, 55, 8551.
- T. Kimura, A. Kato, C. Hotehama, A. Sakuda, A. Hayashi, M. Tatsumisago, Solid State Ionics 2019, 333, 45.
- J. Liang, N. Chen, X. Li, X. Li, K. R. Adair, J. Li, C. Wang, C. Yu, M. Norouzi Banis, L. Zhang, S. Zhao, S. Lu, H. Huang, R. Li, Y. Huang, X. Sun, *Chem. Mater.* 2020, 32, 2664.
- H. Kwak, K. H. Park, D. Han, K. W. Nam, H. Kim, Y. S. Jung, J. Power Sources 2020, 446, 227338.
- G. Liu, X. Sun, X. Yu, W. Weng, J. Yang, D. Zhou, R. Xiao, L. Chen, X. Yao, *Chem. Eng. J.* 2021, 420, 127692.
- Z. Zhang, J. Zhang, Y. Sun, H. Jia, L. Peng, Y. Zhang, J. Xie, J. Energy Chem. 2020, 41, 171.
- M. K. Tufail, L. Zhou, N. Ahmad, R. Chen, M. Faheem, L. Yang, W. Yang, *Chem. Eng. J.* 2021, 407, 127149.
- A. Hayashi, H. Muramatsu, T. Ohtomo, S. Hama, M. Tatsumisago, J. Mater. Chem. A 2013, 1, 6320.
- 28. A. Sakuda, A. Hayashi, M. Tatsumisago, Sci. Rep. 2013, 3, 2261.
- 29. Y. Li, X. Wang, H. Zhou, X. Xing, A. Banerjee, J. Holoubek, H. Liu, Y. S. Meng, P. Liu, *ACS Energy Lett.* **2020**, *5*, 955.
- F. Zhao, S. H. Alahakoon, K. Adair, S. Zhang, W. Xia, W. Li, C. Yu, R. Feng, Y. Hu, J. Liang, X. Lin, Y. Zhao, X. Yang, T. K. Sham, H. Huang, L. Zhang, S. Zhao, S. Lu, Y. Huang, X. Sun, *Adv. Mater.* 2021, 33, 2006577.

#### SUPPORTING INFORMATION

Additional supporting information may be found in the online version of the article at the publisher's website.

**How to cite this article:** X. Lu, O. Camara, Z. Liu, A. Windmüller, C. -L. Tsai, H. Tempel, S. Yu, H. Kungl, R. -A. Eichel, *Electrochem. Sci. Adv.* **2023**, *3*, e2100208. https://doi.org/10.1002/elsa.202100208